ornl

ORNL/TM-12946

OAK RIDGE NATIONAL LABORATORY

MARTIN MARIETTA

RECEIVED
DEC 13 1995
OSTI

Study on Severe Accident Fuel Dispersion Behavior in the Advanced Neutron Source Reactor at Oak Ridge National Laboratory

S. H. Kim
R. P. Taleyarkhan
S. Navarro-Valenti
V. Georgevich

MASTER

MANAGED BY
MARTIN MARIETTA ENERGY SYSTEMS, INC.
FOR THE UNITED STATES
DEPARTMENT OF ENERGY

DISTRIBUTION OF THIS DOCUMENT IS UNLIMITED

This report has been reproduced directly from the best available copy.

Available to DOE and DOE contractors from the Office of Scientific and Technical Information, P.O. Box 62, Oak Ridge, TN 37831; prices available from (615) 576-8401, FTS 626-8401.

Available to the public from the National Technical Information Service, U.S. Department of Commerce, 5285 Port Royal Rd., Springfield, VA 22161.

This report was prepared as an account of work sponsored by an agency of the United States Government. Neither the United States Government nor any agency thereof, nor any of their employees, makes any warranty, express or implied, or assumes any legal liability or responsibility for the accuracy, completeness, or usefulness of any information, apparatus, product, or process disclosed, or represents that its use would not infringe privately owned rights. Reference herein to any specific commercial product, process, or service by trade name, trademark, manufacturer, or otherwise, does not necessarily constitute or imply its endorsement, recommendation, or favoring by the United States Government or any agency thereof. The views and opinions of authors expressed herein do not necessarily state or reflect those of the United States Government or any agency thereof.

DISCLAIMER

Portions of this document may be illegible in electronic image products. Images are produced from the best available original document.

ORNL/TM-12946

ENGINEERING TECHNOLOGY DIVISION

STUDY ON SEVERE ACCIDENT FUEL DISPERSION BEHAVIOR IN THE ADVANCED NEUTRON SOURCE REACTOR AT OAK RIDGE NATIONAL LABORATORY

S.H. Kim
R.P. Taleyarkhan
S. Navarro-Valenti
V. Georgevich

September 1995

Prepared by the
Oak Ridge National Laboratory
Oak Ridge, Tennessee 37831-8045
managed by
LOCKHEED MARTIN ENERGY SYSTEM, INC.
for the
U.S. DEPARTMENT OF ENERGY
under contract DOE-AC05-84OR21400

TABLE OF CONTENTS

Page

Table of Contents ii

List of Tables iii

List of Figures iv

Abstract 1

1 Introduction 1

2 ANS System Description 2

3 Particle Entrainment During a Severe Fuel Damage Event 3

4 Melt Particle Breakup 5

4.1 Initial particle size 5
4.2 Particle size distribution 5
4.3 Effect of melt solidification on melt breakup 6

5 Particle Dispersion Throughout RCS 8

6 Results and Analysis 10

7 Summary and Conclusion 12

8 Nomenclature 16

9 References 16

LIST OF TABLES

page

Table 1 Severe accident characteristics of the ANS and other reactor systems..... 2

Table 2 Discretized Particle Distribution..... 6

Table 3 Eigenvalues for Various Particle Diameters 7

Table 4 Constants for Pilch's Correlation for Melt Breakup Time for Gas-Liquid System 7

LIST OF FIGURES

page

Fig. 1 Fluid velocity at channel exit versus inlet velocity under hypothetical, fixed inlet flow conditions 4

Fig. 2 Melt particle solidification time 8

Fig. 3 Schematic nodalization of ANS RCS 9

Fig. 4(a) Distribution of debris mass upon 100% core disruption 13

Fig. 4(b) Distribution of debris mass upon 100% core disruption 13

Fig. 5 Debris particle distribution from 0.5 to 5.0 s 14

Fig. 6 Debris particle distribution from 0.05 to 0.50 s 14

Fig. 7(a) Time variation of debris mass at selected locations 15

Fig. 7(b) Time variation of debris mass at core downstream 15

Study on Severe Accident Fuel Dispersion Behavior in the Advanced Neutron Source Reactor at Oak Ridge National Laboratory

S.H. Kim, R.P. Taleyarkhan, S. Navarro-Valenti, and V. Georgevich
Engineering Technology Division
Oak Ridge National Laboratory
Oak Ridge, TN 37831-8045

Abstract

Core flow blockage events have been identified as a leading contributor to core damage initiation risk in the Advanced Neutron Source (ANS) reactor. During such an accident, insufficient cooling of the fuel in a few adjacent blocked coolant channels out of several hundred channels, could also result in core heatup and melting under full coolant flow condition in other coolant channels. Coolant inertia forces acting on the melt surface would likely break up the melt into small particles. Under thermal-hydraulic conditions of ANS coolant channel, micro-fine melt particles are expected. Heat transfer between melt particle and coolant, which affects the particle breakup characteristics, was studied. The study indicates that the thermal effect on melt fragmentation seems to be negligible because the time corresponding to the breakup due to hydrodynamic forces is much shorter than the time for the melt surface to solidify. The study included modeling and analyses to predict transient behavior and transport of debris particles throughout the coolant system. The transient model accounts for the surface forces acting on the particle that result from the pressure variation on the surface, inertia, virtual mass, viscous force due to the relative motion of the particle in the coolant, gravitation, and resistance due to inhomogenous coolant velocity radially across piping due to expected turbulent coolant motions. The results indicate that debris particles would reside longest in the heat exchangers because of lower coolant velocity there. Also they are entrained and move together in a cloud.

1 Introduction

The Advanced Neutron Source (ANS) is to be a multipurpose neutron research center and is currently in the advanced conceptual design stage at the Oak Ridge National Laboratory (ORNL). Major areas of research will include condensed matter physics, materials science, isotope production, and fundamental physics [1, 2]. The source of neutrons in the facility is planned to be a 303-MW(t) heavy-water-cooled and moderated research reactor housed in a large, double-walled containment dome and surrounded by thermal neutron beam experimental facilities. The reactor uses U_3Si_2–Al cermet fuel in a plate-type configuration. Cooling systems are designed with many safety features, including large heat sinks sufficient for decay heat removal; passive inventory control by accumulators, pools, and flooded cells; a layout that maximizes natural circulation capabilities; and fast, redundant shutdown systems. A defense-in-depth philosophy has been adopted. In response to this commitment, ANS project management initiated severe accident analyses and related technology development early in the design phase. This was done to aid in designing a sufficiently robust containment for retention and controlled release of radionuclides in the event of an accident. It also provides a means for satisfying on- and off-site regulatory requirements, accident-related dose exposures, containment response, and source-term best-estimate analyses for Level-2 and -3 Probabilistic Risk Analyses (PRAs) that will be produced.

Moreover, it will provide the best possible understanding of the ANS under severe accident conditions and, consequently, provide insights for development of strategies and design philosophies for accident mitigation, management, and emergency preparedness efforts [3].

Past scoping studies have indicated the possibility of core debris recriticality in reactor coolant system (RCS) piping sections, in a dispersed configuration [4]. Clearly, in order to provide the basis for closure of this concern and the incorporation of suitable design fixes if necessary, the likelihood of such dispersed configurations needs to be quantified. This requires an ability to describe the various material motions and the characterization of the various energetic phenomena as they are affected by phase change and/or fission gas release.

In this paper, the modeling and analysis framework for evaluation of ANS core debris dispersion phenomena are described. For an accident initiated by a core flow blockage event, several mathematical models have been developed for characterizing debris particles, statistical distribution of particle size, dispersion, and transport into the coolant stream. These models are presented along with analyses results conducted to date.

2 ANS System Description

The ANS is currently in the conceptual design stage. As such, design features of the containment and reactor systems are evolving, based on insights from ongoing studies. Table 1 summarizes the current principal design features of the ANS from a severe accident perspective compared with the High Flux Isotope Reactor (HFIR) and a commercial light-water reactor (LWR). Specifically, the ANS reactor will use uranium silicide fuel in an aluminum matrix with plate-type geometry and a total core mass of about 100 kg. The power density of the ANS will be only about 2 times higher than that of the HFIR, but about 50 to 100 times higher than that of a large LWR. Because of such radical differences, high-power-density research reactors may give rise to significantly different severe accident issues. Such considerations have led to increased attention being given to phenomenological considerations dealing with steam explosions, recriticality, core-concrete interactions, core-melt progression, and fission-product release. However, compared to power reactor scenarios, overall containment loads from hydrogen generation and deflagration are relatively small for the ANS.

Table 1 Severe accident characteristics of the ANS and other reactor systems

Parameter	Commercial LWR	HFIR	ANS
Power, MW(t)	2600	100 [a]	303
Fuel	UO_2	U_3O_8–Al	U_3Si_2–Al
Enrichment (m/o)	2–5	93	93 [b]
Fuel cladding	Zircaloy	Al	Al
Coolant/moderator	H_2O	H_2O	D_2O
Coolant outlet temperature, K	590	342	365
Average power density, MW/L	<0.1	2.0	4.5
Clad melting temperature, K	2123	853	853
Hydrogen generation potential, kg	850	10	12

[a] Currently operating at a reduced power of 85 MW.

[b] 1992 baseline (reduced enrichment fuel, in a larger core, now being considered)

The reactor core is enclosed within a core pressure boundary tube and enveloped in a reflector vessel, which is immersed in a large pool of light water. Each element of the core is constructed with a series of involute fuel plates arranged in an annular array. The involute design provides uniform coolant gaps at all spanwise positions. Each 1.27-mm-thick fuel plate consists of 0.254-mm-thick 6061 aluminum cladding material, sandwiching a 0.762-mm mixture of uranium silicide (U_3Si_2) and aluminum. Each coolant gap is also 1.27 mm in width and has a span of 70.29 or 87.35 mm (upper or lower core, respectively). Fuel plates are welded to inner and outer cylindrical side plates with each element having 507 mm of fueled length. Unheated 10-mm leading and trailing edges complete the fuel plate design.

3 Particle Entrainment During a Severe Fuel Damage Event

Accident progression to the onset of core melting due to flow blockage is described in a companion paper [5]. Once a fuel plate becomes molten, structural change is expected to occur due to the presence of the unstable interfaces. Generally, the interaction at an interface between two media of different densities results in wave formation. Stability of this interface largely depends on surface tension and coolant inertia forces ($\sigma/\delta_l \sim \rho u^2$). In most cases of interest, a characteristic length, δ_l, can be related to the critical wave length as

$$\delta_l \sim \sqrt{\frac{\sigma}{g\,\Delta\rho}} \tag{1}$$

where $\Delta\rho$ is the density difference of two contacting media. Therefore, a critical flow velocity at which the interface becomes unstable, u_e, can be written [6]

$$u_e = \zeta \left[\frac{\sigma_p\, g\,(\rho_p - \rho_c)}{\rho_c^2}\right]^{0.25} \tag{2}$$

where the subscripts, p, c denote the molten fuel plate and coolant medium, respectively, and ρ_c is the density of the continuous phase for a given stable regime (e.g., coolant). At a liquid water-vapor interface, the first waves to appear are small ripples. Higher vapor velocities lead to an increase in the amplitude of these ripples, and soon three-dimensional disturbances are generated. For a two-phase system of liquid water and vapor, it was observed experimentally that the water liquid film abruptly broke up and was entrained by the vapor at the critical vapor velocity, corresponding to the stability number (ζ) of around 3.7 [7]. There is uncertainty in applying this stability number for a liquid-liquid interface. However, it provides us with an idea about the critical velocity at which the fuel entrainment would occur.

Using Eq. (2) for the ANS, the critical coolant velocity for the fuel entrainment can be obtained as 1.3 m/s (based on ρ_c = 1,000 kg/m^3, ρ_p = 2,700 kg/m^3, σ_p = 0.868 N/m). If the coolant is saturated steam, then 13 m/s is the velocity obtained based on ρ_c = 12 kg/m^3 at 2.5 MPa.

To examine the coolant condition further (in a single channel where significant boiling is assumed to occur under a hypothetical severe accident), its velocity is evaluated as a function of channel inlet velocity assuming constant pressure and homogeneous two-

phase flow. By neglecting internal heat generation and viscous dissipation, the local steam velocity at any axial position, z, is given by [8]

$$u_g(t) = \frac{G_i(t)}{\rho_c} + \Omega[z - \lambda(t)] \tag{3}$$

the parameter, Ω, represents the speed at which phase change takes place and is expressed as

$$\Omega \equiv \frac{2\dot{q}'' w v_{fg}}{h_{fg} A_{x-s}} \tag{4}$$

The boiling boundary, λ(t), is given by

$$\lambda(t) = \frac{G_i(t) A_{x-s} \Delta h_{sub}}{2\dot{q}'' w} \tag{5}$$

Figure 1 illustrates fluid velocity at the channel exit (0.507 m) as a function of fluid inlet velocity for various heat fluxes. As the inlet velocity increases, the exit velocity decreases because of increased boiling boundary length. The exit velocity eventually reaches the same value as the inlet velocity when no bulk boiling occurs in the channel (due to the assumption of constant pressure). In reality, since we have several hundred channels in parallel, the occurrence of significant boiling in any one channel would cause parallel channel flow instability [5], which results in flow from the channel with boiling to be diverted into other non-boiling channels. Nevertheless, as seen in the figure, fluid velocity in the coolant channel is sufficiently high to entrain the fuel melt whether or not it boils.

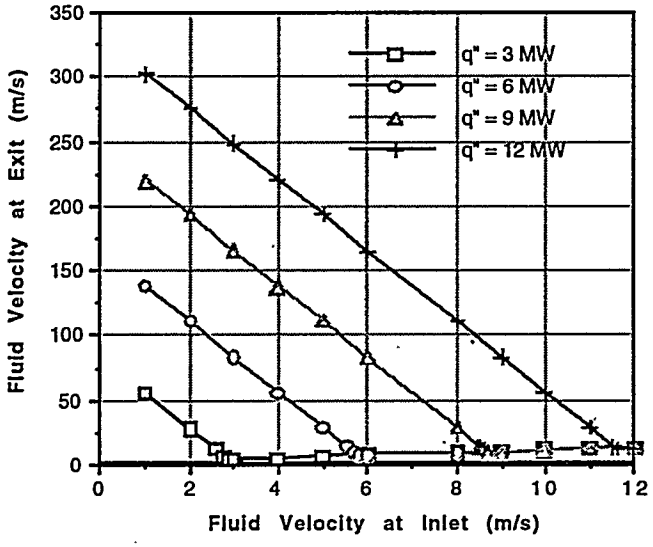

Fig. 1 Fluid velocity at channel exit versus inlet velocity under hypothetical, fixed inlet flow conditions

4 Melt Particle Breakup

4.1 Initial particle size

The characteristic length, defined in Eq. (1), is based on an instability at the interface induced by the density difference of two contacting media. For aluminum, Eq. (1) gives values of 5 to 7 mm depending on vapor or liquid phase of continuing fluid medium. This number is substantially larger than the physical thickness of a fuel plate (e.g., 1.27 mm) and of the coolant gap. Initial breakup of the melted plate is thought to be governed by Kelvin-Helmholtz (KH) instability. A wave is developed at the interface of two media moving at different velocities. An intact (but molten) plate with coolant (either vapor or liquid) flowing at a relatively high velocity in ANS conditions is a configuration similar to melt jet penetrating through a stagnant (or slowly moving) water pool. Extensive research has been performed in the past to predict this jet penetration problem. A general agreement is that at the interface between melted jet and water, KH instability determines the jet breakup behavior. Kocamustafaogullari derived the maximum stable particle size based on classical KH instability theory for molten drops, and his predictions were compared reasonably well against breakup data collected by several other researchers for various gas-liquid and liquid-liquid systems [9]. According to his predictions and data collected, the maximum stable particle size varies in the range of 5 to 10 mm for a gas-liquid system and of 6 to 150 mm for a liquid-liquid system. Initial particle sizes must have been larger than these maximum particle sizes. As indicated above, however, initial breakup will be limited by the physical size of the melted plate. Furthermore, any wave growth at the melt-coolant interface must be limited by the physical size of the coolant gap, which is 1.27 mm. Therefore, in our study, we assume that the initial melt particle is 1.27-mm-diameter, which is the plate thickness, instead of expending further efforts to study details of interfacial stability problems.

4.2 Particle size distribution

Based on Wolfe's extensive data collected for Bis drops (d_0 = 1.6 mm, 2.7 mm), Pilch described particle size variations as a log-normal distribution given as [10]

$$f\left(\frac{d}{d_o}\right)=\frac{1}{\sqrt{2\pi}}\frac{1}{\beta}\frac{d_o}{d}\exp\left\{-\frac{1}{2\beta^2}\left[\ln\left(\frac{d}{d_o}\right)-\gamma\right]^2\right\} \qquad (6)$$

where β and γ can be determined from Wolfe's data as a function of the Weber number as

$$\beta = -0.0879\ln(We)+1.38 \qquad \text{and} \qquad \gamma=\ln(-0.168\,We^{-0.5}) \qquad (7)$$

The normalized number distribution in Eq. (6) is defined as the fractional number of fragments per drop per normalized size range. Our molten debris consists of aluminum mixed with uranium silicide, and thus the statistical distribution of particle size might be different from the Wolfe's data. Furthermore, a chemical reaction between aluminum and uranium silicide at the temperature above aluminum melting temperature may change the material properties due to eutectic formation. Such a change in material properties has not been studied yet. For the current study, therefore, it was decided to use the Wolfe's data for particle size distribution. In future, we can probably collect our own data for our material, and formulate similar expressions for β and γ, as given in Eq. (7). For our

condition, assuming 2700 kg/m^3 for debris density, 20 m/s for liquid coolant velocity, and 1.27 mm for initial particle diameter, the Weber number is estimated as 585. Listed in Table 2 is the resulting particle distribution discretized into five bins.

Table 2 Discretized Particle Distribution

Bin	Size range, diam. (m)	Number fraction	Mass fraction
1	10^{-8} to 5 x 10^{-6}	0.47923	0.10999
2	5 x 10^{-6} to 7 x 10^{-6}	0.2232	0.23645
3	7 x 10^{-6} to 9 x 10^{-6}	0.1832	0.34797
4	9 x 10^{-6} to 10^{-5}	0.07699	0.1973
5	10^{-5} to 10^{-4}	0.03748	0.10829

4.3 Effect of melt solidification on melt breakup

While the melt (or melted plate) undergoes breakup, the particles will transfer heat to its surrounding medium. Under certain conditions, the particle breakup process may be limited by solidification of particles. Such a thermal effect is assessed by comparing the time for the melt to become solidified against the time for melt breakup to occur.

The melt particles will start to solidify if heat generation becomes less than heat losses. A solid crust will form at the particle surface and grow inward. As it grows, this crust shell becomes stronger; at the same time it will be exposed to increased stress because of pressure buildup due to heat generation inside of the crust shell. At a certain threshold shell thickness, the crust will break up, and the internal melt will be exposed to hydrodynamic forces for further breakup. The time for this thermal process (t_t) can be characterized into two periods. One is the time taken for the temperature of the melt particle surface to decrease to its solidification temperature (t_{ts}), and the other is the time taken for the crust shell to break up due to internal pressure buildup (t_{tb}). The effect of this thermal process can be assessed by comparing this time against the time for the melt breakup due to hydrodynamic forces (t_h). If $t_{ts} >> t_h$, evaluation of t_{tb} is not necessary, and we can conclude that hydrodynamics dominate over thermal process for melt particle breakup.

To evaluate t_{ts}, transient heat conduction equation for a sphere is written as

$$\frac{1}{\alpha}\frac{\partial\theta}{\partial t}=\frac{1}{r^2}\frac{\partial}{\partial r}\left(r^2\frac{\partial\theta}{\partial r}\right)+\frac{\dot{q}'''}{k} \tag{8}$$

where $\theta = T - T_\infty$, and T_∞ is the surrounding bulk temperature. With boundary and initial conditions as the following,

$$\left.\frac{\partial\theta}{\partial r}\right|_{r=0}=0,\quad -k\left.\frac{\partial\theta}{\partial r}\right|_{r=R_p}=h\theta,\quad \theta|_{t=0}=T_o-T_\infty\equiv\theta_o \tag{9}$$

Equation (8) can be solved to give the temperature distribution in a melt particle as

$$\theta(r,t)=\frac{1}{r}\sum_{n=1}^{\infty}k_n\sin(\lambda_n r)e^{-\alpha\lambda_n^2 t}+\frac{\dot{q}'''}{6k}(R_p^2-r^2)+\frac{\dot{q}'''R_p}{3h} \tag{10}$$

where the constant k_n is determined as a function of the eigenvalue, λ_n. Table 3 lists the four eigenvalues for various particle diameters with 740 W/m^2-K of convection heat transfer coefficient and 190 W/m-K of thermal conductivity. The first term on the right-hand side of Eq. (10) becomes zero for n = 1 ($\lambda_1 = 0$). For n = 3,4,..., this term becomes too small to compare with that for n = 2, due to the large eigenvalues in the exponential term.

Table 3 Eigenvalues for Various Particle Diameters (d)

n	d = 4 x 10^{-4} m	d = 8 x 10^{-4} m	d = 1.27 x 10^{-3} m
1	0	0	0
2	241.6	170.8	135.6
3	22,467	11,234	7,077
4	38,626	19,313	12,166

When the melt starts to solidify at its surface, therefore, the corresponding time can be approximated from Eq. (10) as

$$t_{ts} \approx -\frac{1}{\alpha\lambda_2^2}\ln\left[\frac{R_p\left(\theta_m - \frac{\dot{q}'''R_p}{3h}\right)}{k_2\sin(\lambda_2 R_p)}\right], \quad where\,\theta_m = T_{melt} - T_\infty \tag{11}$$

Hydrodynamic breakup time (t_h) is defined as the time when the melt particles are no longer subject to further breakup. The normalized breakup time was correlated by Pilch, based on experimental data collected by several investigators for a gas-liquid system, and given as [10]

$$\tau_h = a(We - 12)^b \tag{12}$$

Hydrodynamic breakup time is defined from normalized breakup time as

$$t_h = \tau_h \frac{d_o}{u_c - u_p}\left(\frac{\rho_c}{\rho_p}\right)^{0.5} \tag{13}$$

The constants a and b in Eq. (12) are listed in Table 4.

Table 4 Constants for Pilch's Correlation for Melt Breakup Time for Gas-Liquid System

Range	a	b
12 ≤ We < 18	6	- 0.25
18 ≤ We < 45	2.45	0.25
45 ≤ We < 351	14.1	- 0.25
351 ≤ We < 2670	0.766	0.25
2670 ≤ We	5.5	0

There are not enough data available to draw a general conclusion for the breakup time for the liquid-liquid system. Baines' study of the breakup of mercury drops in water revealed a normalized breakup time for the liquid-liquid system, τ_b, of 4 to 5, which is comparable to that for a gas-liquid system [11] . On the other hand, Theofanous reported a significantly lower breakup time for a mercury-water system (e.g., 2 to 5 times faster) [12]. However, if the breakup time from Eq. (12) is estimated to be smaller than the solidification time, t_s, we can still draw a reasonable conclusion that the hydrodynamics govern the melt break-up process.

With 1.27 mm of initial diameter, the breakup time given by Eqs. (12) and (13) is estimated to be 0.145 ms. Melt solidification time is illustrated in Fig. 2, as a function of particle size for various levels of power generation and 10 K initial super heat above the particle melting temperature. One can easily see that the particle breakup due to hydrodynamic process occurs much earlier, even before the melt surface starts to become solidified. This leads to the conclusion that the particle breakup process is mainly governed by hydrodynamic process, at least in the fuel melting accidents in the ANS, which we currently consider.

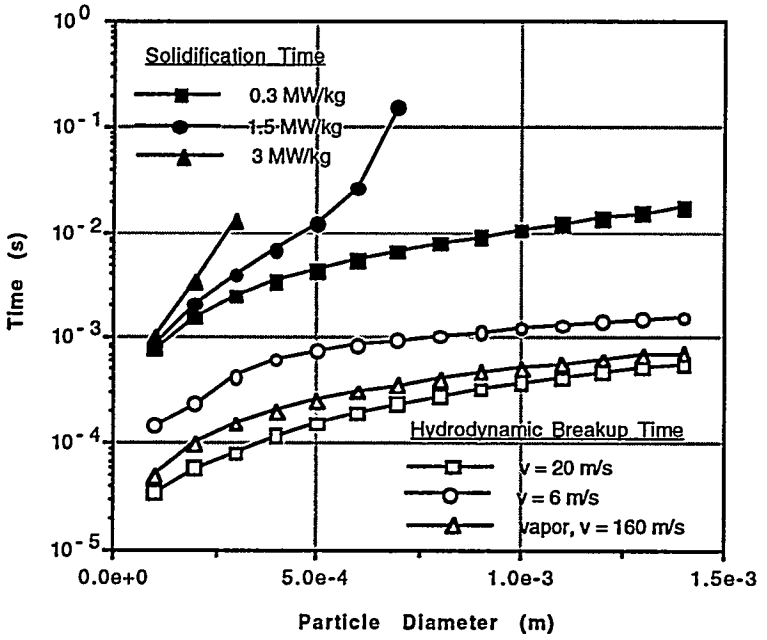

Fig. 2 Melt particle solidification time

5 Particle Dispersion Throughout RCS

It is desirable to know how debris particles originating from the core region in a severe accident would be dispersed throughout the coolant system at different velocities. To conduct this evaluation, the entire coolant system was nodalized into several control volumes, as seen in Fig. 3. Particle density of size bin-i in control volume-j, $n_{i,j}$ can then be expressed as

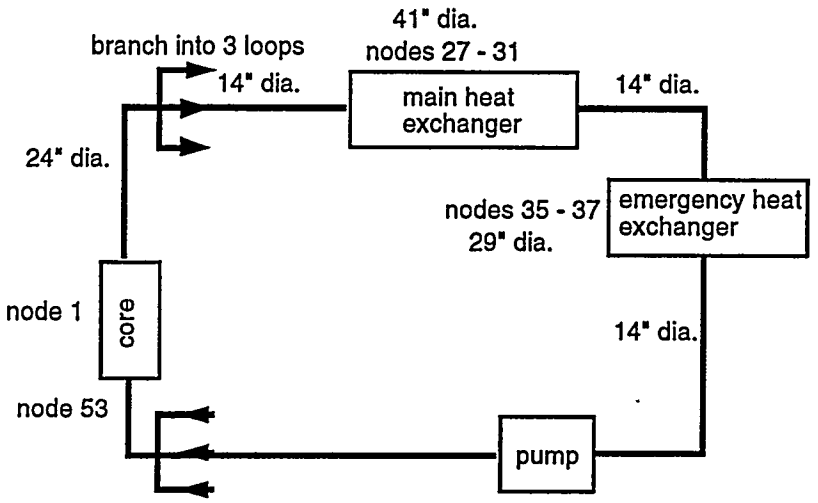

Fig. 3 Schematic nodalization of ANS RCS

$$\frac{dn_{i,j}}{dt} = \frac{1}{V_j}\left[n_{i,j}\, u_{i,j}\, A_j\right]_{out}^{in} + s_{i,j} \tag{14}$$

where the bracket, $[\ ]_{out}^{in}$, represents inflow subtracted by outflow and where donor cell properties are used for flow properties, including particle velocity and particle density.

It is realized that the motion of particles in the coolant stream is certainly nonuniform, and always changing both in direction and magnitude of velocity. However, to obtain an overall perspective and to capture the essential physics of the transport processes, a one-dimensional approximation was made. The transient rectilinear motion of a spherical particle in a turbulent flow, with nonzero mean velocity, can be given as [13,14]

$$\begin{aligned}\frac{\pi d^3\rho_p}{6}\frac{du_p}{dt} = \frac{\pi d^3\rho_c}{6}\frac{du_c}{dt} + \frac{1}{2}\frac{\pi d^3\rho_c}{6}\left(\frac{du_c}{dt} - \frac{du_p}{dt}\right) + 3\pi\nu_c\rho_c d\left(u_c - u_p\right) \\ + \frac{\pi d^3}{6}\left(\rho_c - \rho_p\right)g\delta - \frac{5\pi d^3\rho_c}{16R}u_c\left(u_c - u_p\right)\end{aligned} \tag{15}$$

where ν is the kinematic viscosity and subscripts p and c are particle and coolant fluid, respectively. The first term on the right-hand side of Eq. (15) is the surface force acting on the particle that results from the pressure variation on the surface, which is a function of the pressure field in the entraining coolant. The second term is for the inertia of the virtual mass (entrained with relative motion of the particle in the coolant) and is equivalent to an increase in particle mass equal to half the mass of the coolant displaced. The third term describes the viscous force (e.g., Stokes' linear resistance) due to the relative motion of the particle in the coolant. The fourth term is the gravitational force, and δ in this term is the directional cosine. The last term describes a resistance due to inhomogeneous coolant motion caused by turbulence. According to Tchen [14], coolant motion in the radial direction in pipe flow induces additional resistance to the particle movement and is expressed as

$$F = \frac{\pi}{4}\rho_c d^3\left(u_c - u_p\right)\frac{\partial u_c}{\partial r} \tag{16}$$

For turbulent flow in a round pipe, the coolant velocity profile can be approximated as [15]

$$u_c(r) = u_{c,\max}\left(1 - \frac{r}{R}\right)^{\frac{1}{7}} \tag{17}$$

Averaging the derivative of Eq. (17) with respect to r for $u_{c,max} = 5u_c/4$ yields

$$\left\langle \frac{\partial u_c}{\partial r} \right\rangle = \frac{1}{R}\int_0^R \frac{\partial u_c}{\partial r}\, dr = -\frac{5}{4}\frac{u_c}{R} \tag{18}$$

Therefore, Eq. (16) averaged over a pipe cross-sectional area is expressed as the last term in Eq. (15).

Interactions between particles, and between particles and pipe (or structure) wall, are not included in Eq. (15) because particle sizes under consideration are small enough to neglect particle collision. The coolant velocity is assumed to be constant with time in our calculations and is taken from a separate RELAP calculation (i.e., 25 m/s in core and 6~7 m/s in other regions of the reactor coolant loop). This implies the absence of any significant influence of debris particles on the bulk coolant flow. This postulate was based on the significantly larger inertia of the bulk coolant flow relative to inertia of debris particles.

6 Results and Analysis

A preliminary calculation has been performed to observe the debris particle dispersion throughout the primary RCS for a very simplistic case; a postulated adiabatic heatup and melting at the whole core. The entire coolant system was nodalized into 53 control volumes. Each control volume was set at about 2 m in length. The effective core diameter (e.g., control volume 1) was determined from the rate of coolant flowing through the core (1,994 kg/s) and the coolant density of 1,000 kg/m^3. Among the four coolant loops, three loops are normally on-line, with the fourth loop on a standby basis. The control volumes 16 through 52 represent one of the three loops. One main heat exchanger and one emergency heat exchanger are in each coolant loop. The primary coolant is to flow through the shell side of each heat exchanger. Main and emergency heat exchangers are represented by five and three control volumes, respectively; that is, control volumes 27 through 31 for main heat exchanger and 35 through 37 for emergency heat exchanger, as seen in Fig. 3. The control volume length and coolant velocity for the heat exchangers were obtained to correctly evaluate the residence time of the coolant in heat exchangers. For the given coolant velocity (e.g., 0.78 m/s for main heat exchangers, and 1.57 m/s for emergency heat exchangers) and mass flow rate, the diameter of each heat exchanger was calculated as 1.04 m (41 in.) and 0.73 m (28.9 in.) for main and emergency heat exchangers, respectively.

Only the first control volume representing the reactor core generates debris particles. For a test case, the debris particles were generated at the rate of 667.67 kg/s for 0.15 s, which results in 100 kg of debris particles. This 667.67 kg/s was based on a constant adiabatic melting of the core; that is 303 MW of power divided by 0.397 MJ/kg of latent heat of fusion of aluminum. Actually it gives 755.67 kg/s and 0.1323 s of melting period to generate 100 kg of debris particles. However, the melting rate was adjusted to be 667.67 kg/s during 0.15 s of melting period. The statistical distribution of the particle size is

given in Table 2. Note that the largest particle size would be (as in Table 2) 10^{-4} m, which is even smaller than the mesh size of the strainer in the cold leg. Therefore, it is conservatively assumed that the effect of the strainer for capturing the core debris particles is negligible. Variation in particle size turns out not to affect the debris dispersion behavior very much because the high coolant velocity leads the particle to approach the terminal velocity (i.e., coolant velocity) very quickly. It was usually observed that the particles reach the coolant velocity within the first control volume where they are introduced. Core debris is a mixture of solid uranium silicide particles dispersed in molten aluminum. Because uranium silicide is heavier than aluminum (e.g., 12.8 g/ml for U_3Si_2 vs 2.7 g/ml for Al), it is possible for U_3Si_2 particles to be segregated. To examine this possibility, calculations were performed as if all the particles are U_3Si_2. The resulting particle distribution throughout the coolant system was compared with that for the case with all aluminum particles. The differences were almost negligible because the particles reach the equilibrium velocity so quickly in the fast-moving coolant that we consider here. Therefore, the description of results and the analysis are provided for the dispersion of aluminum particles.

Figures 4 through 7 demonstrate the results in terms of debris mass and also the temporal variation of debris mass at a few selected locations. Debris mass distributions at several different times are shown in Figures 4 (a) and (b). It is seen that the heat exchangers are the locations where the particles reside longest. One must note that debris mass in one actual coolant loop is to be one-third of the value shown in the figures for nodes from 16 through 52. Also, it needs to be pointed out that a particle takes about 27 s to traverse an entire coolant loop, as evident in Figure 4 (b) for the debris mass at 30, 35 and 40 s. Figure 5 shows the same results for an earlier time period, from 0.5 s through 5 s. It is clearly seen that the debris mass at the moving front diminishes as the particles disperse farther. Debris mass is also shown in Figure 6 for 0.05 s through 0.5 s. It is seen that the debris particle mass in the control volume 1 (core) increases during debris particle generation (0.15 s). In this calculation, one should note that the intact core mass is not included as a part of debris mass in the control volume 1, which is the core. Upon completing debris particle production, core debris mass decreases as seen in the figure. However, debris mass in the next volume (CV-2) keeps increasing to about 90 kg for a time because the particle takes about 0.28 s to travel through the control volume as evident from the fact that the particle starts showing up in the third volume at 0.3 s in the figure (this time difference, 0.28 s vs 0.3 s is due to the finite size of time step). Figures 7 (a) and (b) show the temporal variation of debris mass at control volumes 2,3,4, and two heat exchanger volumes. It is seen that at the coolant downstream out of the core, maximum debris mass is predicted to be about 90 kg. This means that the entire core moves almost together under the assumed conditions of debris particle generation and introduction into the fast-moving coolant. However, it shows that the debris particles disperse throughout the coolant loop volumes as they move. The entire debris mass (100 kg) is seen to stay in the main heat exchanger at around 14 s. But, one must recall that we have three heat exchangers holding this 100 kg of core mass. Therefore, the main heat exchanger in each coolant loop would hold one-third of 100 kg of debris mass if debris at the branch node 16 is equally distributed among the three loops. To check the sensitivity of nodalization on the debris mass, the control volume 2 was further divided into two volumes. The results indicate that the control volume nodalization does not seem to be very sensitive in debris dispersion, while it may be possible to have locally higher debris concentration in some instances.

7 Summary and Conclusion

In this paper, models for debris particle dispersion have been developed and presented. Along with particle dispersion, debris breakup behavior was also characterized. The transient model for particle dispersion and transport accounts for the surface forces acting on the particle that results from the pressure variation on the surface, inertia, virtual mass, viscous force due to the relative motion of the particle in the coolant, gravitation, and resistance due to inhomogenous coolant velocity radially across piping due to possible turbulent coolant motions. Numerical calculations were performed for debris dispersion throughout the primary coolant system for a postulated adiabatic heatup and melting of the core..

Coolant inertia force acting on the melt surface will likely break up the melt into small particles. Under the expected thermal-hydraulic conditions in an ANS coolant channel, micro-fine melt particles are predicted. Heat transfer between melt particles and coolant, which affects the particle breakup characteristics, was studied. The study indicated that the thermal effect on melt fragmentation seems to be negligible because the time corresponding to the breakup due to hydrodynamic forces is much shorter than the time for the melt surface to solidify. For the specific case analyzed, the results of particle dispersion calculations indicate that debris particles would reside longest in heat exchangers because of the lower coolant velocity there. Also, core debris tends to move together upon melting and entrainment. Recriticality concerns could be studied in future, by coupling the breakup and transport models developed here with realistic severe accident scenarios and core melt progression models.

The current model for the debris dispersion does not account for the interaction between particles, or for interaction between particles and structure walls, which may slow down the particle dispersion in some degree. However, further work to include particle interaction modeling does not seem to be necessary at this stage because its effect is thought to be small. Also missing from the current model is the feedback to the coolant. The coolant velocity must be affected by existence of debris in its stream. The current model, however, assumes that the coolant velocity stays constant, unaltered by debris particles in it stream. In addition, the model for the particle entrapment in local pockets where the bulk coolant velocity is nearly zero is missing.

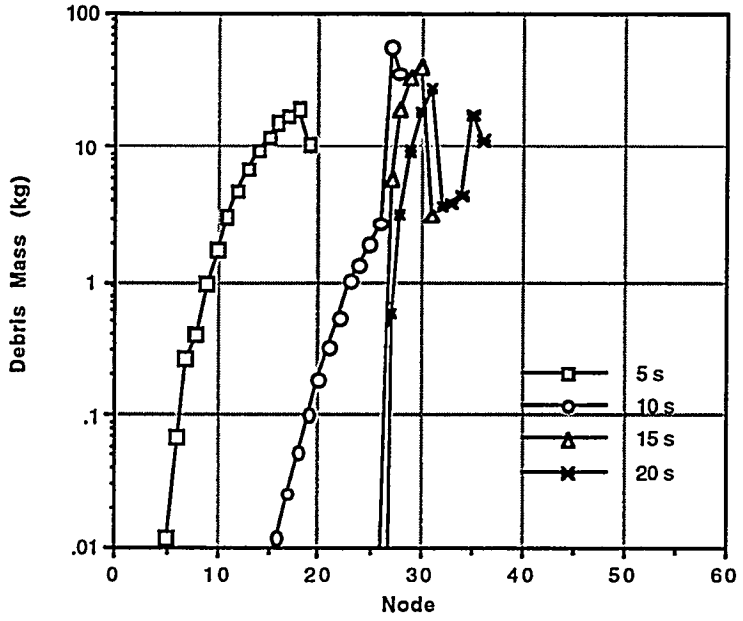

Fig. 4(a) Distribution of debris mass upon 100% core disruption

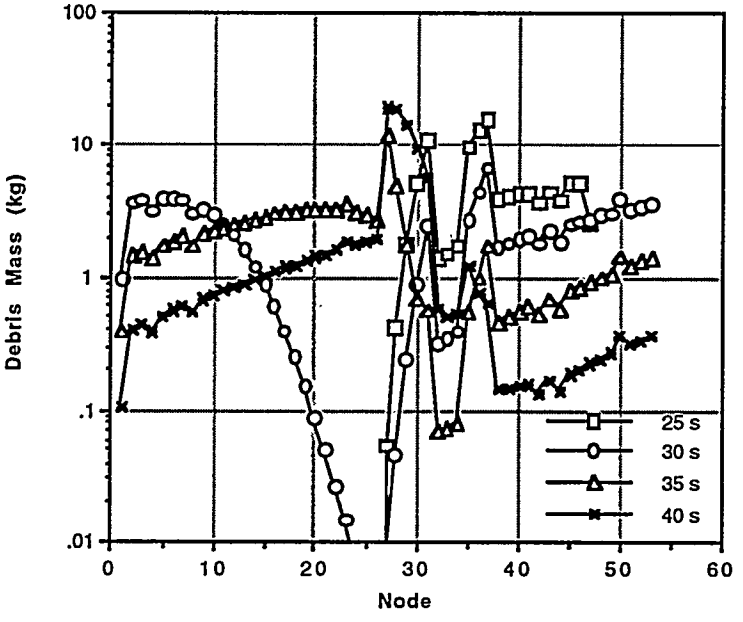

Fig. 4(b) Distribution of debris mass upon 100% core disruption

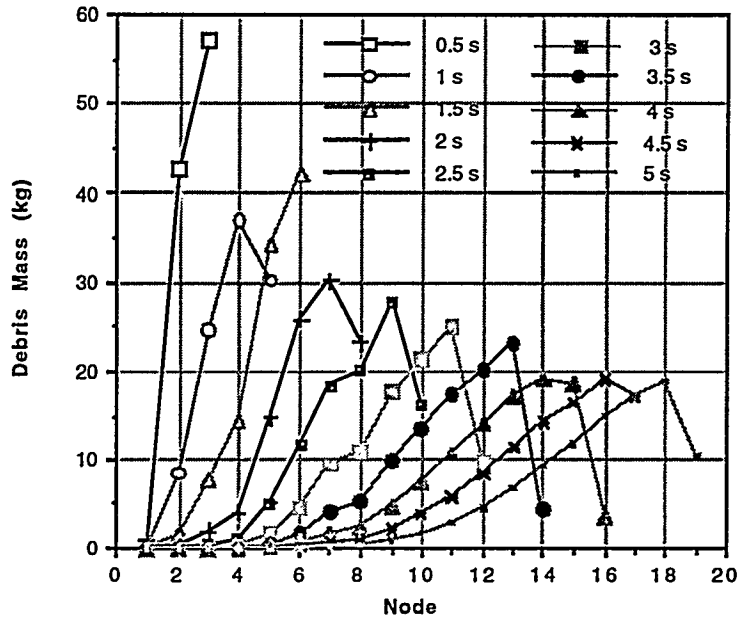

Fig. 5 Debris particle distribution from 0.5 to 5.0 s

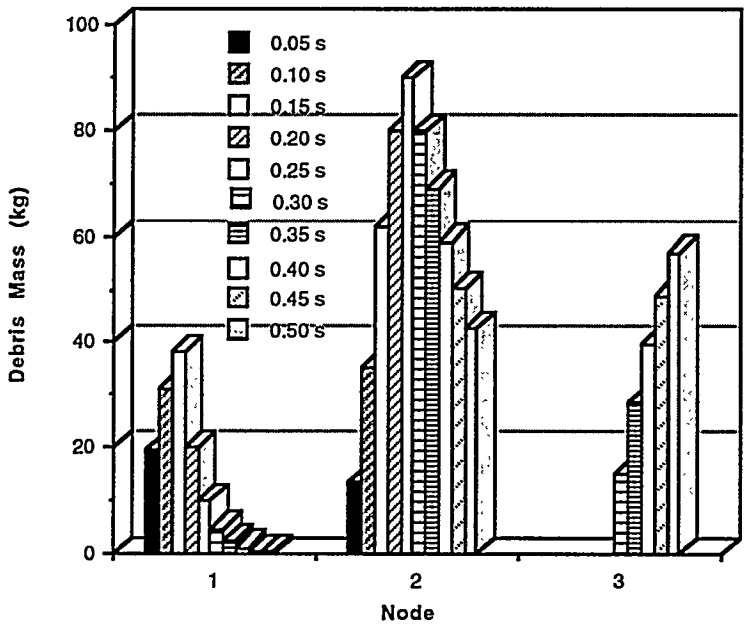

Fig. 6 Debris particle distribution from 0.05 to 0.50 s

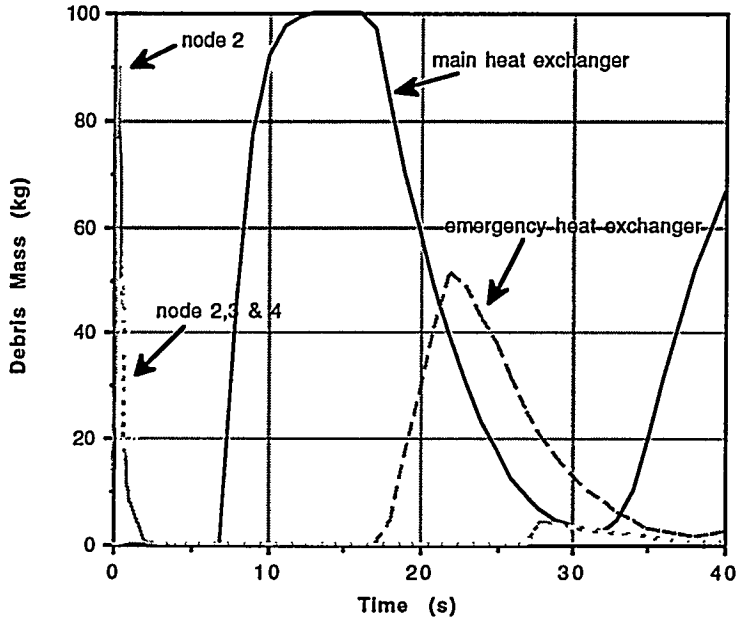

Fig. 7(a) Time variation of debris mass at selected locations

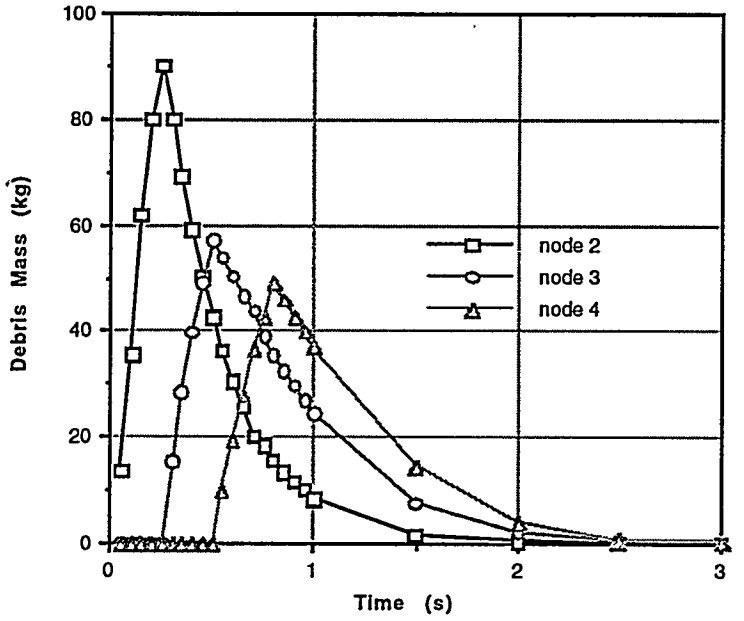

Fig. 7(b) Time variation of debris mass at core downstream

8 Nomenclature

A_j	cross-sectional flow area of control volume j
A_{x-s}	cross-sectional area
d	particle diameter
d_o	initial particle diameter
G_i	mass flux at channel inlet
g	gravitational acceleration
h	convective heat transfer coefficient
h_{fg}	heat of vaporization of water
k	thermal conductivity
n_{ij}	number density of particle bin i in control volume j
q"	heat flux
q'''	volumetric heat generation
R	pipe radius or effective radius of control volume
R_p	melt particle radius
s_{ij}	rate of volumetric particle source of bin i in control volume j
T	temperature
t_h	particle break-up time due to hydrodanamic process
t_t	particle break-up time due to thermal process
t_{ts}	time taken for the particle surface to be solidified
t_{tb}	time taken for the solidified particle shell to be broken up
u	velocity
u_{ij}	particle velocity of bin i in control volume j
v_{fg}	difference of specific volumes (= v_g - v_f)
V_j	volume of control volume j
w	channel width
We	Weber number ($=\rho u^2 d_o/\sigma$)
z	channel length
Δh_{sub}	inlet subcooling of coolant channel

α	thermal diffusivity
β & γ	experimentally determined coefficients for particle distribution
δ	directional cosine
δ_l	characteristic length
λ	boiling boundary
λ_n	eigenvalue
ν	kinematic viscosity
ρ	material density
σ	surface tension
ζ	stability number
Ω	phase change speed

9 References

[1] C. D. West, "The Advanced Neutron Source: A New Reactor-Based Facility for Neutron Research," Trans. Amer. Nuc. Soc. 61, 375 (June 1990).

[2] C. D. West, "Advanced Neutron Source Plant Design Requirements," ORNL/TM-11625, (May 1992).

[3] R. P. Taleyarkhan, and S. H. Kim, "Severe Accident Risk Minimization Studies for the Advanced Neutron Source at the Oak Ridge National Laboratory," Proc. of the 5th International Workshop on Containment Integrity, Washington, D.C. (May 1992).

[4] S.H. Kim et al., "Modeling and Analysis of Core Debris Recriticality During Hypothetical Severe Accidents in the Advanced Neutron Source Reactor," Proc. of the Second International Conference on Nuclear Engineering (ICONE-2), San Francisco, CA (March 1993).

[5] S.H. Kim et al., "Modeling and Analysis Framework for Core Damage Propagation During Flow-Blockage Initiated Accidents in the Advanced Neutron Source Reactor at Oak Ridge National Laboratory," Proc. of the 7th International Meeting on Nuclear Hydraulics (NURETH-7), Saratoga Springs, NY (September 1995).

[6] G.B. Wallis, One-Dimensional Two-Phase Flow, McGraw-Hill Book Co. (1969).

[7] M. Ishii and M.A. Grolmes, "Inception Criteria for Droplet Entrainment in Two-phase Cocurrent Film Flow," AIChE Journal, 21(2), 308 (March 1975).

[8] R .T. Lahey,Jr., and F.J. Moody, The Thermal-Hydraulics of a Boiling Water Nuclear Reactor, an ANS monograph (1977).

[9] G. Kocamustafaogullari, I.Y. Chen, and M. Ishii, "Unified Theory for Predicting Maximum Fluid Particle Size for Drops and Bubbles," NUREG/CR-4028 (October 1984).

[10] M. Pilch, C.A. Erdman, and A.B. Reynolds, "Acceleration Induced Fragmentation of Liquid Drops," NUREG/CR-2247 (August 1981).

[11] M. Baines and N.E. Buttery, "Differential Velocity Fragmentation in Liquid-Liquid Systems," RD/B/N4643, Berkley Nuclear Laboratories (September 1979).

[12] T.G. Theofanous et al., "LWR and HTGR Coolant Dynamics: The Containment of Severe Accidents," NUREG/CR-3306 (July 1983).

[13] N.P. Cheremisinoff, and R. Gupta, Handbook of Fluids in Motion, Ann Arbor Science (1983).

[14] C.-M. Tchen, "Mean Value and Correlation Problems Connected with the Motion of Small Particles Suspended in a Turbulent Fluid," Mededeling No. 51 Uit Het Laboratorium Voor Aero-En Hydrodynamica Der Technische Hogeschool Te Delft, Martinus Nijhoff (1947) .

[15] R.B. Bird et al., Transport Phenomena, John Wiley & Sons (1960).

Internal Distribution List

1.	D. H. Cook	12.	L. J. Ott
2.	W. G. Craddick	13.	D. L. Selby
3.	E. C. Fox	14.	D. B. Simpson
4.	V. Georgevich	15-17.	R. P. Taleyarkhan
5.	S. R. Greene	18.	C. D. West
6.	R. M. Harrington	19.	ORNL Patent Section
7.	S. A. Hodge	20.	Central Research Library
8-10.	S. H. Kim	21-22	Laboratory Records Department
11.	R. H. Morris		

External Distribution

23 S. Navarro-Valenti, 16 River Street #2, South Natick, MA 01760
24 J. Close, Idaho National Laboratories, P.O. Box 1625, EG&G, Idaho Falls, Idaho 83415
25. M. L. Corradini, Department of Nuclear Engineering, 1500 Johnson Drive, University of Wisconsin, Madison, Wisconsin, 53706-1687
26. M. L. Hyder, SRTC, Westinghouse Savannah River, Co., 1991 South Centennial Avenue, Bldg. 1, Aiken, South Carolina, 29803
27. R. T. Lahey, Nuclear Engineering and Engineering Physics, Rensselaer Polytechnic Institute, JEC 5048, Troy, New York, 12180-3590
28. M. Z. Podowoski, Nuclear Engineering and Engineering Physics, Rensselaer Polytechnic Institute, JEC 5048, Troy, New York, 12180-3590
29. J. Rsyskamp, Idaho National Laboratories, P.O. Box 1625, EG&G, Idaho Falls, Idaho 83415
30 -31. DOE, Office of Scientific and Technical Information, P.O. Box 62, Oak Ridge, Tennessee 37831
32. Sung-Tack Shin, KIDA, Chongryang P.O. Box 250, Togondae-mun-gu, Seoul, 130-650, South Korea
33. Kun-Joong Yoo, KAERI, P.O. Box 105, Yusung-gu, 305-600, South Korea
34. Tom King, U.S. Nuclear Regulatory Commission, MS T10-E37, Washington, D.C. 20555
35. Joe Donaghue, U. S. Nuclear Regulatory Commission, Washington, D. C. 20555
36. A. Drozd, U.S. Nuclear Regulatory Commission, Washington, D.C. 20555
37. T. Fuketa, Japan Atomic Energy Research Institute, Takai-Mura, Ibaraki-Ken, 319-11 Japan
38. J. Sugimoto,
39. T. G. Theofanous, University of California at Santa Barbara, Department of Chemical & Nuclear Engineering, Santa Barbara, California 93106